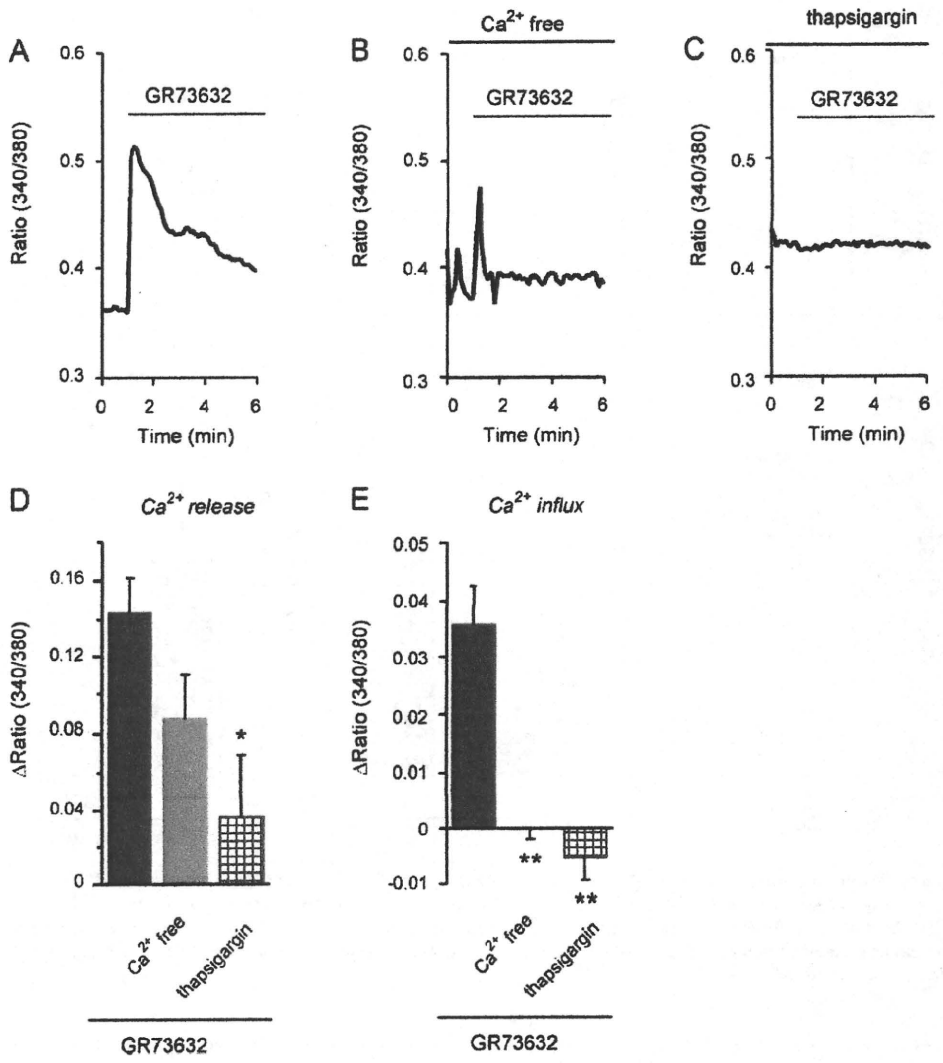

Fig. 4. Influence of both Ca^{2+} store and extracellular Ca^{2+} on the GR73632-induced increase in $[Ca^{2+}]_i$ in spinal astrocytes. The trace in each graph (A–C) shows the representative mean $[Ca^{2+}]_i$ in randomly selected cells. The fura-2-loaded cells were treated with 1000 nM of GR73632 in the presence (A) or absence (B and C) of Ca^{2+} in Hanks' buffer, respectively. After pre-treatment with 1 μM of thapsigargin (C) for 20 min in Ca^{2+}-free Hanks' buffer, the cells were stimulated with GR73632. The extent of Ca^{2+} release from intracellular Ca^{2+} stores induced by GR73632 was quantified by determining the differences between the ratio (340/380) of the basal and the peak level obtained after GR73632 treatment (D). The extent of the extracellular Ca^{2+} influx induced by GR73632 was quantified by determining the differences between the ratio (340/380) of the basal level and the level at 2 min after a peak $[Ca^{2+}]_i$ (E). The data are expressed as the means ± S.E.M. (*bars*) of separate experiments. $^{*}p < 0.05$, $^{**}p < 0.01$ in comparison with the value for the cells treated with GR73632 alone.

channels, or Pyr3 (3 μM), a selective TRPC3 antagonist (Kiyonaka et al., 2009) inhibited only the transient increase of $[Ca^{2+}]_i$ as shown in Fig. 8A–C. Quantitative analysis data confirmed that these inhibitors completely inhibited the GR73632-mediated influx of extracellular Ca^{2+} without affecting the release of Ca^{2+} from intracellular Ca^{2+} stores (Fig. 8D and E). Furthermore, we found by immunofluorescence that the immunostaining for TRPC3 was co-localized with that of GFAP (Fig. 7B–D), thus indicating that TRPC3 is mostly expressed in the plasma membrane of spinal astrocytes. These findings suggest that the NK-1 receptor-stimulated extracellular Ca^{2+} influx might be mediated by TRPC3.

As mentioned above, PKC was thought to participate in the influx of extracellular Ca^{2+}. To confirm this hypothesis, further investigation was preformed to elucidate the relationship between PKC and TRPC channels. Co-treatment with either BTP2 or Pyr3 and BIM completely inhibited the GR73632-indeuced in $[Ca^{2+}]_i$ (Fig. 9A–D). Quantitative data indicated that not only BTP2, but also Pyr3, significantly blocked the GR73632-induced Ca^{2+} influx by BIM (Fig. 9E and F). Taken together, these data suggest that the GR73632-induced influx of extracellular Ca^{2+} through TRPC3 is negatively regulated by PKC.

4. Discussion

In this study, we found that SP evoked an increase in $[Ca^{2+}]_i$ in spinal astrocytes by the activation of PLC and the IP_3 receptor through the NK-1 receptor. This increase in $[Ca^{2+}]_i$ by stimulation of the NK-1 receptor was composed of both Ca^{2+} release from IP_3-sensitive intracellular Ca^{2+} store and extracellular Ca^{2+} influx through TRPC channels. Furthermore, we found that the former was positively modulated by PKA, and the latter was negatively regulated by PKC.

In our study, CP-96345 (a NK-1 receptor antagonist) was the most effective compound found to inhibit the SP-induced increase in $[Ca^{2+}]_i$. We also demonstrated that the NK-1 receptor is expressed in spinal astrocytes by staining with an NK-1 receptor antibody.

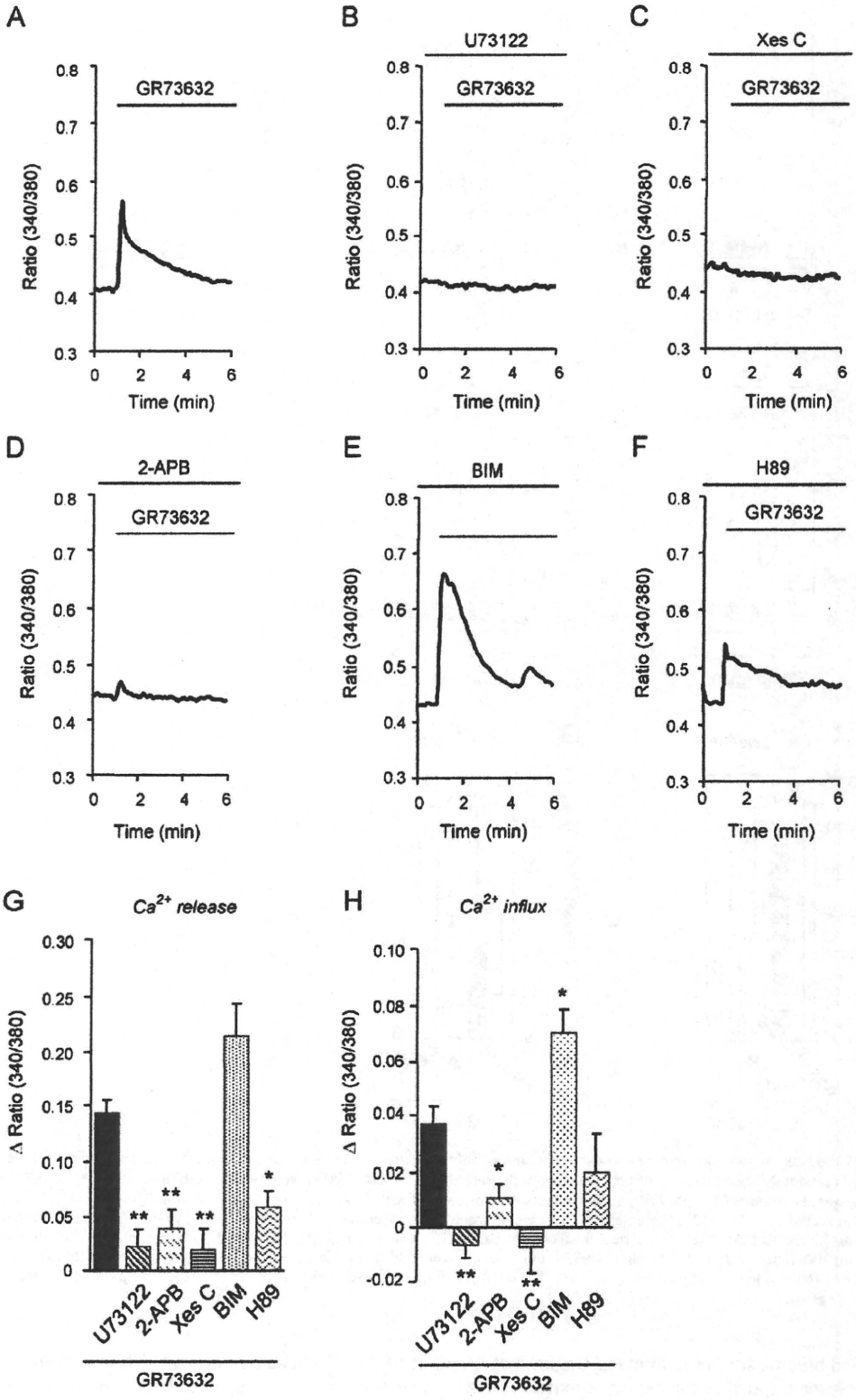

Fig. 5. Effects of inhibitors of several intracellular signaling molecules on the GR73632-induced increase in $[Ca^{2+}]_i$ in spinal astrocytes. The trace in each graph (A–F) shows the representative mean of $[Ca^{2+}]_i$ in randomly selected cells. The fura-2-loaded cells were treated with 1000 nM of GR73632 in Hanks' buffer (A–F). After the cells were pretreated with 10 μM U73122 (B), 1 μM xestospongin C (Xes C) (C), 100 μM 2-APB (D), 10 μM BIM (E) or 10 μM H89 (F) for 20 min, they were stimulated with GR73632. The extent of Ca^{2+} release from the intracellular Ca^{2+} stores induced by GR73632 was quantified by determining the differences between the ratio (340/380) of the basal and the peak level obtained after GR73632 treatment (G). The extent of extracellular Ca^{2+} influx induced by GR73632 was quantified by determining the differences between the ratio (340/380) of the basal level and the level at 2 min after a peak $[Ca^{2+}]_i$ (H). The data are expressed as the means ± S.E.M. (*bars*) of separate experiments. $^{*}p < 0.05$, $^{**}p < 0.01$ in comparison with the value for the cells treated with GR73632 alone.

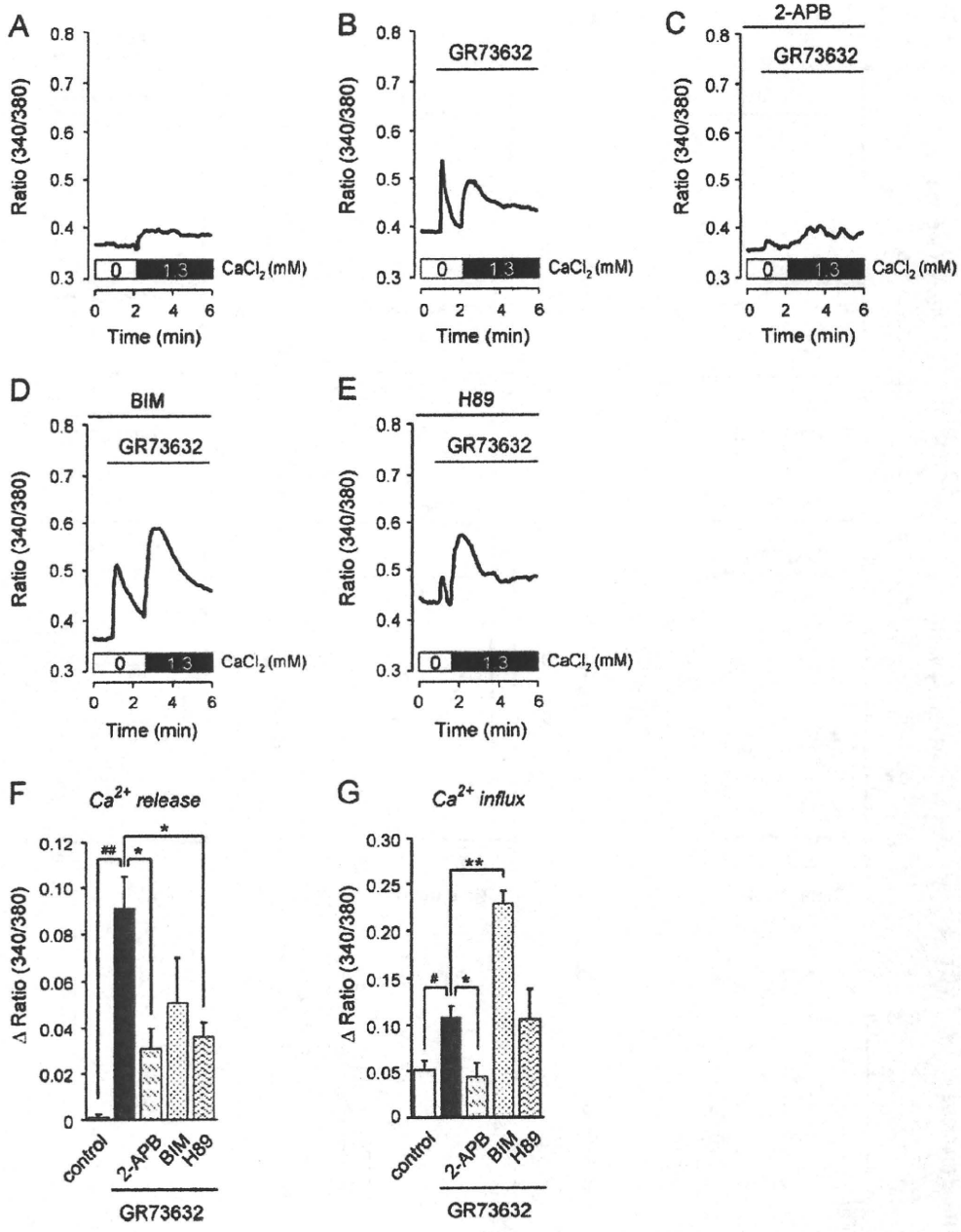

Fig. 6. Effects of 2-APB, BIM and H89 on both Ca^{2+} release and extracellular Ca^{2+} influx induced by GR73632 in spinal astrocytes. The trace in each graph (A–E) shows the representative mean $[Ca^{2+}]_i$ in randomly selected cells. The fura-2-loaded cells were either untreated (A) or were treated with (B–E) 1000 nM of GR73632 in Ca^{2+}-free Hanks' buffer, followed by the subsequent addition of 1.3 mM $CaCl_2$. After the cells were pretreated with 100 μM 2-APB (C), 10 μM BIM (D) or 10 μM H89 (E) for 20 min in Ca^{2+}-free Hanks' buffer, they were stimulated with GR73632. The extent of Ca^{2+} release from the intracellular Ca^{2+} stores induced by GR73632 was quantified by determining the differences between the ratio (340/380) of the basal and the peak level obtained after GR73632 treatment (G). The extent of extracellular Ca^{2+} influx induced by GR73632 was quantified by determining the differences between the ratio (340/380) of the level before addition of $CaCl_2$ and the peak level obtained after the addition (H). The data are expressed as the means ± S.E.M. (*bars*) of separate experiments. $^{\#}p < 0.05$, $^{\#\#}p < 0.01$ in comparison with the value for control. $^{*}p < 0.05$, $^{**}p < 0.01$ in comparison with the value for the cells treated with GR73632 alone.

According to radioligand binding studies in humans, the level of SP binding to the NK-1 receptor in spinal astrocytes was about six times that in brain astrocytes (Palma et al., 1997). Indeed, even 100 nM of SP did not have any effect on $[Ca^{2+}]_i$ in brain astrocytes (data not shown). Therefore, we would conclude that the SP-NK-1 receptor interaction might be strongly involved in the regulation of spinal astroglial functions, including $[Ca^{2+}]_i$ mobilization in the spinal cord. Moreover, GR73632, a selective NK-1 agonist which did not affect either NK-2 or -3 receptors (Maggi, 1995), was used to reveal the mechanisms of the NK-1 receptor-stimulated increase in $[Ca^{2+}]_i$ of spinal astrocyte in the present study. Hagan et al. (1991) and Meini et al. (1995) have demonstrated that GR73632 possess a higher constrictive effect than SP in both the rat urinary bladder and the guinea-pig trachea. In this study, however, the extent of Ca^{2+} response evoked by 1000 nM GR73632 was as same as that by 10 nM SP, indicating that a hundredfold dose of GR73632 is need to mimic the Ca^{2+} response by SP. In addition, there was a tendency for GR94800 (a NK-2 receptor antagonist) and SB222200 (a NK3 receptor antagonist) to attenuate the SP-evoked increase in $[Ca^{2+}]_i$. These data show the possibility that the SP-induced increase in $[Ca^{2+}]_i$ is involved in NK-2 and -3 receptors, although NK-1 receptor plays the most important role for its action in spinal astrocytes.

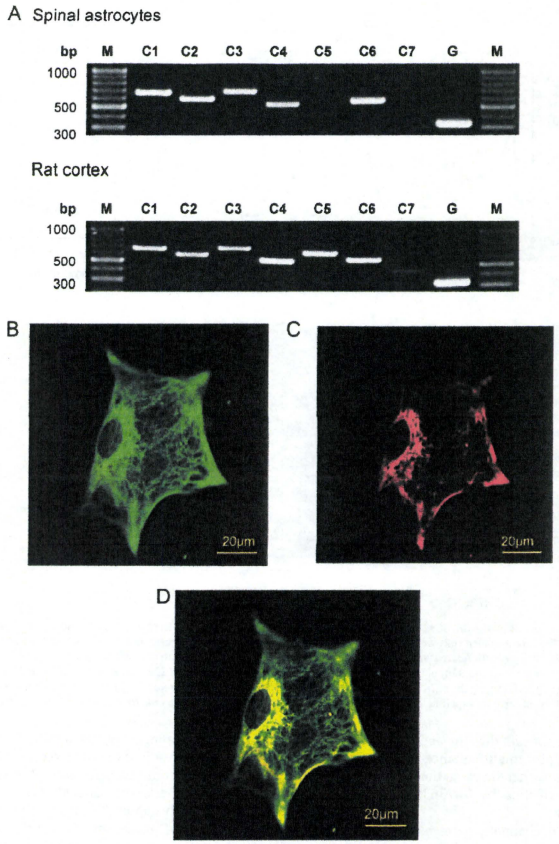

Fig. 7. TRPC3 is expressed in cultured spinal astrocytes. (A) RT-PCR analysis of TRPC channels mRNA expression in cultured rat spinal astrocytes. Each lane represents the cDNA fragments of TRPC1–7 (C1–C7) and GAPDH (G) amplified from the RNA of cultured spinal astrocytes (the upper panel) or rat cortex (the lower panel), respectively. The sizes of fragments and sequences of primers used are indicated in Table 1. The products of PCR from rat cortex are shown as a positive control. Lane M indicates the size marker. (B–D) An immunofluorescence analysis of GFAP (green; B) and TRPC3 (red; C) expression in cultured spinal astrocytes. The expression of TRPC3 was found in GFAP-labeled cells (D).

In this study, U73122 completely attenuated the GR73623-treated increase of $[Ca^{2+}]_i$ in spinal astrocytes, thus suggesting that PLC activation is indispensable for the increase in $[Ca^{2+}]_i$ initiated by stimulation of the NK-1 receptor. In addition, inhibitory effects of thapsigargin and xestospongin C on the GR73632-induced increase in $[Ca^{2+}]_i$ indicates that IP_3-sensitive intracellular Ca^{2+} stores are involved in the increase of $[Ca^{2+}]_i$ initiated by stimulation of the NK-1 receptor. These data suggest that GR73632 could produce IP_3 by the activation of PLC, which then triggers Ca^{2+} release through the IP_3 receptor expressed on Ca^{2+} stores. This is in agreement with a previous report by Palma et al. (1997) who showed that SP caused accumulation of IP_3 in spinal astrocytes.

Furthermore, Holst et al. (2001) demonstrated that not only Gq, but also Gs, proteins are associated with the NK1 receptor, and that the cAMP-PKA cascade contributes to these receptor-mediated functions. In fact, we elucidated that PKA regulates the GR73632-induced Ca^{2+} release (Figs. 4F and 5D), although the present study did not clarify how PKA modulated the Ca^{2+} release through the IP_3 receptor. Bezprozvanny (2005) or Volpe and Alderson-Lang (1990) reported that the activation of PKA enhanced the Ca^{2+} release from IP_3-sensitive Ca^{2+} stores. Furthermore, the IP_3 receptor possesses sites that are phosphorylated by PKA. Mutation of these sites attenuated Ca^{2+} release from IP_3-sensitive Ca^{2+} stores (Wagner et al., 2008). Therefore, these findings suggest that the phosphorylation of the IP_3 receptor by PKA would affect the sensitivity of the

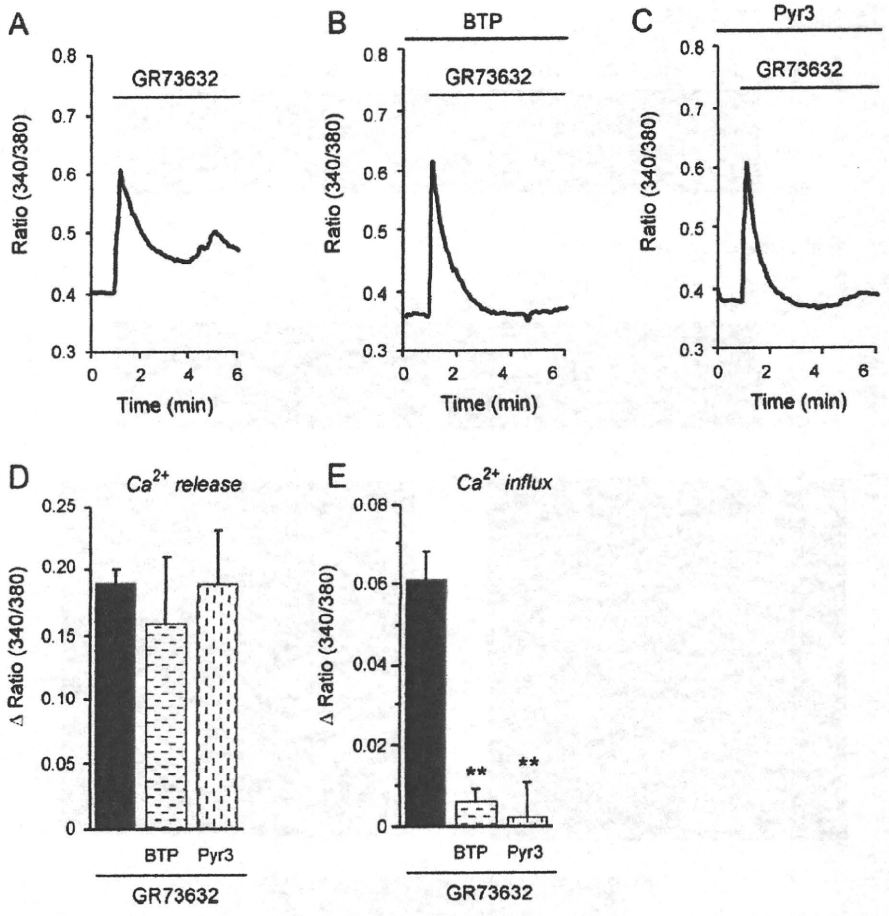

Fig. 8. Effects of inhibitors of TRPC channels on the GR73632-induced increase in $[Ca^{2+}]_i$ by spinal astrocytes. The trace in each graph (A–C) shows the representative mean $[Ca^{2+}]_i$ in randomly selected cells. The fura-2-loaded cells were treated with 1000 nM of GR73632 in Hanks' buffer (A–C). After the cells were pretreated with 10 μM BTP2 (BTP) (B) or 3 μM Pyr3 (C) for 20 min, they were stimulated with GR73632. The extent of Ca^{2+} release from the intracellular Ca^{2+} stores induced by GR73632 was quantified by determining the differences between the ratio (340/380) of the basal and the peak level obtained after GR73632 treatment (D). The extent of the extracellular Ca^{2+} influx induced by GR73632 was quantified by determining the differences between the ratio (340/380) of the basal level and the level at 2 min after a peak of $[Ca^{2+}]_i$ (E). The data are expressed as the means ± S.E.M. (*bars*) of separate experiments. $^{**}p < 0.01$ in comparison with the value for the cells treated with GR73632 alone.

receptor. Taken together, it appears that the activation of PKA by stimulation of the NK1 receptor might enhance the sensitivity of the IP_3 receptor. However, further investigations are needed to determine whether PKA activation by GR73632 leads to phosphorylation of the IP_3 receptor.

In terms of TRPC cation channels, extracellular Ca^{2+} influx through the TRPC channels is known to mainly occur through two pathways: (1) influx induced by depletion of intracellular Ca^{2+} stores (capacitative Ca^{2+} entry: CCE); (2) DAG-sensitive influx (non-CCE: NCCE) (Large et al., 2009). Therefore, TRPC channels are divided into two types (Venkatachalam and Montell, 2007; Large et al., 2009). The DAG-insensitive channels, which are associated with CCE, include TRPC1, 4 and 5. The others are DAG-sensitive channels, and include TRPC2, 3, 6 and 7.

To the best of our knowledge, there have been no previous reports about either the expression or activity of the TRPC channels in spinal astrocytes. The present study is the first to demonstrate that spinal astrocytes express TRPC1, 3, 4 and 6 (Fig. 6) and that Pyr3, which is a selective TRPC3 antagonist (Kiyonaka et al., 2009), completely suppressed the GR73632-induced influx of extracellular Ca^{2+} without affecting GR73632-induced Ca^{2+} release from intracellular Ca^{2+} stores. The inhibitory effects of Pyr3 on the Ca^{2+} influx were similar to those of BTP2 (Fig. 7B and C). Based on these data, we concluded that (1) activation of TRPC3 is responsible for the Ca^{2+} influx induced after the stimulation of the NK-1 receptor, because the 3 μM Pyr3 used in this study had no effect on the activity of other types of TRPC channels (Kiyonaka et al., 2009); (2) the increase in $[Ca^{2+}]_i$ by stimulation of the NK-1 receptor is due to CCE, because xestospongin C completely inhibited the GR73632-induced Ca^{2+} influx. Our hypothesis is consistent with recent reports showing that TRPC3 can not only induce CCE through the IP_3 receptor, but can also function as non-DAG-sensitive channels (Venkatachalam et al., 2003; Woodard et al., 2010). Furthermore, a recent report indicated that TRPC6 evokes CCE by associating with TRPC1, suggesting that DAG-sensitive TRPC channels are involved in not only NCCE, but also CCE (Jardin et al., 2009). Further investigations are needed to better characterize TRPC3 in spinal astrocytes.

In the present study, the BIM-potentiated increase in $[Ca^{2+}]_i$ after stimulation with GR73632 was completely inhibited by Pyr3 suggesting that PKC regulates the activity of TRPC3. Trebak et al. (2005) demonstrated that NCCE induced by OAG, a membrane-permeability analogue of DAG, was suppressed by phosphorylation of Ser^{712} in TRPC3. In addition, they showed that a mutation at Ser^{712} in TRPC3 potentiated the influx of extracellular Ca^{2+} caused by methacholine, an agonist of the muscarinic acetylcholine receptor (Trebak et al., 2005). These findings suggest that the phosphorylation of TRPC3 by PKC is crucial for inhibition of extracellular Ca^{2+} influx. Thus, the activation of TRPC3 after stimulation of the NK-1 receptor might be negatively regulated by the simultaneous activation of PKC.

In conclusion, stimulation of the NK-1 receptor causes Ca^{2+} release from IP_3-sensitive intracellular Ca^{2+} stores via PLC activation, and thereby induces the influx of extracelluar Ca^{2+}

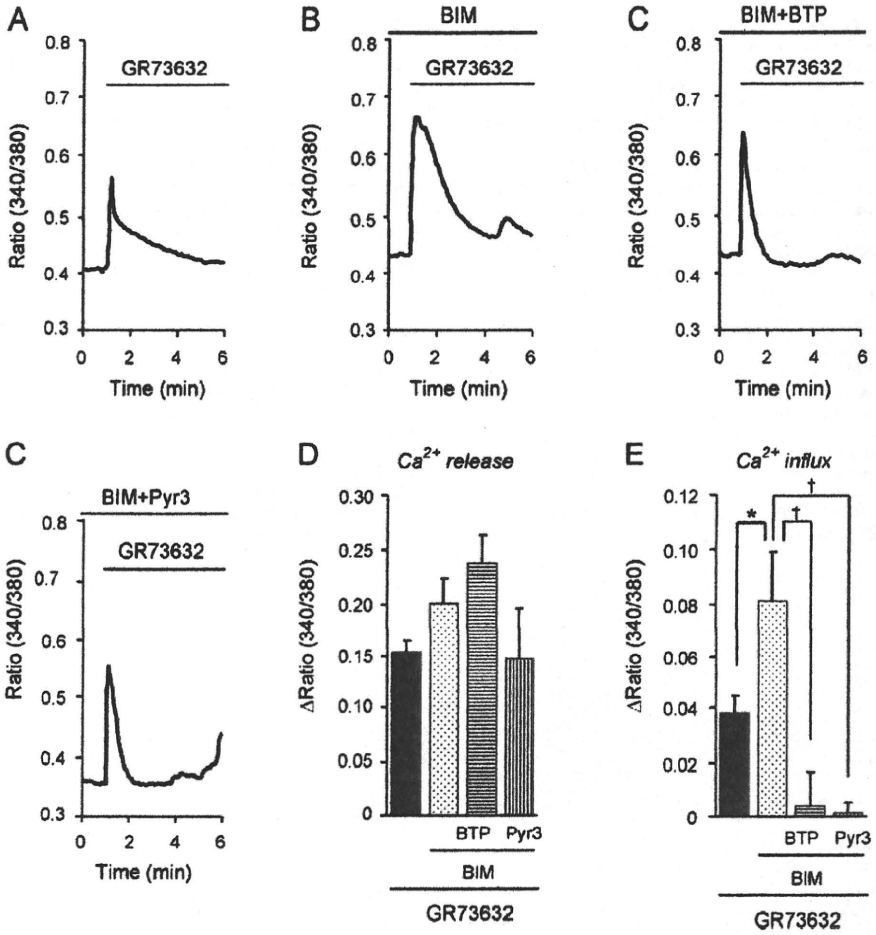

Fig. 9. Involvement of PKC in the GR73632-induced increase in $[Ca^{2+}]_i$ through TRPC channels in spinal astrocytes. The trace in each graph (A–D) shows the representative mean $[Ca^{2+}]_i$ in randomly selected cells. The fura-2-loaded cells were treated with 1000 nM of GR73632 (GR) in Hanks' buffer (A–D). After the cells were pretreated with 10 μM BIM (B), a combination of 10 μM of BIM and BTP2 (BIM + BTP) (C) or 10 μM BIM and 3 μM Pyr3 (BIM + Pyr3) (D) for 20 min, they were stimulated with GR73632. The extent of Ca^{2+} release from the intracellular Ca^{2+} stores induced by GR73632 was quantified by determining the differences between the ratio (340/380) of the basal and the peak level obtained after GR73632 treatment (E). The extent of the extracellular Ca^{2+} influx induced by GR73632 was quantified by determining the differences between the ratio (340/380) of the basal level and the level at 2 min after a peak of $[Ca^{2+}]_i$ (F). The data are expressed as the means ± S.E.M. (*bars*) of separate experiments. $^*p < 0.05$ in comparison with the value for the cells treated with GR73632 alone. $^\dagger p < 0.05$ in comparison with the value for the cells pretreated with BIM + GR73632.

through the TRPC3 in spinal astorcytes. In addition, PKA activation by SP potentiates Ca^{2+} release, while PKC down-regulates the Ca^{2+} influx through TRPC3. Our results indicate that SP binding to the NK-1 receptor in not only neurons but also in spinal astrocytes plays an essential role in spinal synaptic transmission. As a result, these observations provide valuable new insights into the regulation of pain transduction.

Acknowledgements

This study was supported by a Grant-in-Aid for Scientific Research from the Japan Society for the Promotion of Science (JSPS) to Nakata (No. 21590280) and the Japanese Smoking Research Association. We thank Dr. Brian Quinn (Kyushu University, Japan) for his critical reading of the manuscript. We also thank the Analysis Center of Life Science, Hiroshima University for the use of an Argus Hisca color image processor.

References

Barajas, M., Andrade, A., Hernandez-Hernandez, O., Felix, R., Arias-Montano, J.A., 2008. Histamine-induced Ca^{2+} entry in human astocytoma U373 MG cells: evidence for involvement of store-operated channels. J. Neurosci. Res. 86, 3456–3468.

Bezprozvanny, I., 2005. The inositol 1,4,5-triphosphate receptors. Cell Calcium 38, 261–272.

Fields, R.D., Stevens-Graham, B., 2002. New insights into neuron-glia communication. Science 298, 556–562.

Hagan, R.M., Ireland, S.J., Jordan, C.C., Beresford, I.J.M., Deal, M.J., Ward, P., 1991. Receptor-selective, peptidase-resistant agonists at neurokinin NK-1 and NK-2 receptors: new tools for investigating neurokinin function. Neuropeptides 19, 127–135.

Hirota, N., Kuraishi, Y., Hino, Y., Sato, Y., Satoh, M., Takagi, H., 1985. Met-enkephalin and morphine but not dynorphin inhibit noxious stimuli-induced release of substance P from rabbit dorsal horn in situ. Neuropharmacology 24, 567–570.

Holst, B., Hastrup, H., Raffetseder, U., Martini, L., Schwartz, T.W., 2001. Two active molecular phenotypes of the tachykinin NK1 receptor revealed by G-protein functions and mutagenesis. J. Biol. Chem. 276, 19793–19799.

Jardin, I., Gomez, L.J., Salido, G.M., Rosado, J.A., 2009. Dynamic interaction of hTRPC6 with the Orai1-STIM1 complex or hTRPC3 mediates its role in capacitative or non-capacitative Ca^{2+} entry pathway. Biochem. J. 420, 267–276.

Kiyonaka, S., Kato, K., Nishida, M., Mio, K., Numaga, T., Sawaguchi, Y., Yoshida, T., Wakamori, M., Mori, E., Numata, T., Ishii, M., Takemoto, H., Ojida, A., Watanabe, K., Uemura, A., Kurose, H., Morii, T., Kobayashi, T., Sato, Y., Sato, C., Hamachi, I., Mori, Y., 2009. Selective and direct inhibiton of TRPC3 channels underlies biological activities of a pyrazole compound. Proc. Natl. Acad. Sci. U.S.A. 106, 5400–5405.

Large, W.A., Saleh, S.N., Albert, A.P., 2009. Role of phosphoinositol 4,5-bisphosphate and diacylglycerol in regulating native TRPC channel proteins in vascular smooth muscle. Cell Calcium 45, 574–582.

Maggi, C.A., 1995. The mammalian tachykinin receptors. Gen. Pharmacol. 26, 911–944.

Maggi, C.A., Schwartz, T.W., 1997. The dual nature of the tachykinin NK_1 recetor. TiPS 18, 351–353.

Marriott, D.R., Wilkin, G.P., Wood, J.N., 1991. Substance P-induced release of prostaglandins from astrocytes: regional specialisation and correlation with phosphoinositol metabolism. J. Neurochem. 56, 259–265.

Meini, S., Patacchini, R., Lecci, A., Poulos, C., Rovero, P., Maggi, C.A., 1995. GR73,632 and [Glu(OBzl)^{11}] substance P are selective agonists for the Septide-sensitive tachykinin NK_1 receptor in the rat urinary bladder. Neuropeptides 28, 99–106.

Miyano, K., Tang, H.B., Nakamura, Y., Morioka, N., Inoue, A., Nakata, Y., 2009. Paclitaxel and vinorelbine, evoked the release of substance P from cultured rat dorsal root ganglion cells through different PKC isoform-sensitive ion channels. Neuropharmacology 57, 25–32.

Morioka, N., Tanabe, H., Inoue, A., Dohi, T., Nakata, Y., 2009. Noradrenaline reduces the ATP-stimulated phosphorylation of p38 MAP kinase via β-adrenergic receptors–cAMP–protein kinase A-dependent mechanism in cultured rat spinal microglia. Neurochem. Int. 55, 226–234.

Nakajima, Y., Tsuchida, K., Negishi, M., Ito, S., Nakanishi, S., 1992. Direct linkage of three tachykinin receptors to stimulation of both phosphatidylinositol hydrolysis and cyclic AMP cascades in transfected Chinese hamster ovary cells. J. Biol. Chem. 267, 2437–2442.

Nakao, K., Shirakawa, H., Sugishita, A., Matsutani, I., Niidome, T., Nakagawa, T., Kaneko, S., 2008. Ca^{2+} mobilization mediated by transient receptor potential canonical 3 is associated with thrombin-induced morphological changes in 1321N1 human astrocytoma cells. J. Neurosci. Res. 86, 2722–2732.

Palma, C., Minghetti, L., Astolfi, M., Ambrosini, E., Silberstein, F.C., Manzini, S., Levi, G., Aloisi, F., 1997. Functional characterization of substance P receptors on cultured human spinal cord astrocytes: synergism of substance P with cytokines in inducing interleukin-6 and prostaglandin E2 production. Glia 21, 183–193.

Randic, M., Miletic, V., 1977. Effect of substance P in cat dorsal horn neurons activated by noxious stimuli. Brain Res. 128, 164–169.

Severini, C., Improta, G., Falconieri-Erspamer, G., Salvadori, S., Erspamer, V., 2002. The tachykinin peptide family. Pharmacol. Rev. 54, 285–322.

Snijdelaar, D.G., Dirksen, R., Slappendel, R., Crul, B.J., 2000. Substance P. Eur. J. Pain 4, 121–135.

Trebak, M., Hempel, N., Wedel, B.J., Smyth, J.T., Bird, J.S., Putney Jr., J.W., 2005. Negative regulation of TRPC3 channels by protein kinase C mediated phosphorylation of serine 712. Mol. Pharmacol. 67, 558–563.

Venkatachalam, K., Zheng, F., Gill, D.L., 2003. Regulation of canonical transient receptor potential (TRPC) channel function by diacylglycerol and protein kinase C. J. Biol. Chem. 278, 29031–29040.

Venkatachalam, K., Montell, C., 2007. TRP channels. Annu. Rev. Biochem. 76, 387–417.

Volpe, P., Alderson-Lang, B.H., 1990. Regulation of inositol 1,4,5-trisphosphate-induced Ca^{2+} release. II. Effect of cAMP-dependent protein kinase. Am. J. Physiol. 258, 1086–1091.

Wagner, L.E., Joseph, S.K., Yule, D.I., 2008. Regulation of single inositol 1,4,5-trisphosphate receptor channel activity by protein kinase A phosphorylation. J. Physiol. 586, 3577–3596.

Woodard, G.E., López, J.J., Jardín, I., Salido, G.M., Rosado, J.A., 2010. TRPC3 regulates agonist-stimulated Ca^{2+} mobilization by mediating the interaction between type I inositol 1,4,5-trisphosphate receptor, RACK1 and Orai1. J. Biol. Chem. 285, 8045–8053.

Zhou, H., Iwasaki, H., Nakamura, T., Nakamura, K., Maruyama, T., Hamano, S., Ozaki, S., Mizutani, A., Mikoshiba, T., 2007. 2-Aminoethyl diphenylborinate analogues: selective inhibition for store-operated Ca^{2+} entry. Biochem. Biophys. Res. Commun. 352, 227–282.

J Pharmacol Sci 114, 281 – 291 (2010)

Journal of Pharmacological Sciences

Full Paper

Derived (Mutated)–Types of TRPV6 Channels Elicit Greater Ca^{2+} Influx Into the Cells Than Ancestral-Types of TRPV6: Evidence From *Xenopus* Oocytes and Mammalian Cell Expression System

Yuka Sudo[1,2,3], Kiyotaka Matsuo[2], Tomoyuki Tetsuo[2], Satoshi Tsutsumi[2], Masamichi Ohkura[4], Junichi Nakai[4], and Yasuhito Uezono[1,2,3,*]

Departments of [1]Molecular and Cellular Biology and [2]Pharmacology, Nagasaki University Graduate School of Biomedical Sciences, Nagasaki 852-8523, Japan
[3]Cancer Pathophysiology Division, National Cancer Center Research Institute, Tokyo 104-0045, Japan
[4]Saitama University Brain Science Institute, Saitama 338-8570, Japan

Received June 29, 2010; Accepted August 26, 2010

Abstract. The frequency of the allele containing three derived nonsynonymous SNPs (157C, 378M, 681M) of the gene encoding calcium permeable TRPV6 channels expressed in the intestine has been increased by positive selection in non-African populations. To understand the nature of these SNPs, we compared the properties of Ca^{2+} influx of ancestral (in African populations) and derived-TRPV6 (in non-African populations) channels with electrophysiological, Ca^{2+}-imaging, and morphological methods using both the *Xenopus* oocyte and mammalian cell expression systems. Functional electrophysiological and Ca^{2+}-imaging analyses indicated that the derived-TRPV6 elicited more Ca^{2+} influx than the ancestral one in TRPV6-expressing cells where both channels were equally expressed in the cells. Ca^{2+}-inactivation properties in the ancestral- and derived-TRPV6 were almost the same. Furthermore, fluorescence resonance energy transfer (FRET) analysis showed that both channels have similar multimeric formation properties, suggesting that derived-TRPV6 itself could cause higher Ca^{2+} influx. These findings suggest that populations having derived-TRPV6 in non-African areas may absorb higher Ca^{2+} from the intestine than ancestral-TRPV6 in the African area.

Keywords: TRPV6, calcium channel, fluorescence resonance energy transfer (FRET), electrophysiology

Introduction

The genes encoding the transient receptor potential cation channel subfamily V (vanilloid) members 5 and 6 (*TRPV5* and *TRPV6*) are expressed in a wide variety of tissues, with the highest level found in kidney and intestine, respectively. Both *TRPV5* and *TRPV6* encode six-transmembrane proteins that assemble into homotetramers to form Ca^{2+}-selective membrane pores (Fig. 1) (1 – 3). Main Ca^{2+} balance in the body is regulated by absorption through TRPV6 from the intestine and reabsorption and excretion through TRPV5 from renal tubules (1 – 3). Because TRPV6 is involved in the rate-limiting step of dietary calcium absorption, genetic variation of the TRPV6 gene could affect dietary Ca^{2+} absorption as well as Ca^{2+} balance in the body. In the TRPV6 gene, a pattern of positive selection was observed in a 115-kb region of chromosome 7q34-35, which contains four genes, namely *KEL*, *TRPV5*, *TPRV6*, and *EPHB6* (4 – 6). This positive selection signature was observed in non-African populations but not in Africans (4, 5). In *TRPV6*, three derived nonsynonymous single nucleotide polymorphisms (SNPs) (157C, 378M, 681M) were in almost complete linkage disequilibrium and nearly fixed in non-African populations (see Fig. 1) (4, 6). A recent study indicated that the rate of TRPV6 protein evolution is significantly accelerated in the human lineage, but only for a haplotype comprised of a set of derived alleles at

*Corresponding author. uezonoy0404@me.com
Published online in J-STAGE on October 8, 2010 (in advance)
doi: 10.1254/jphs.10169FP

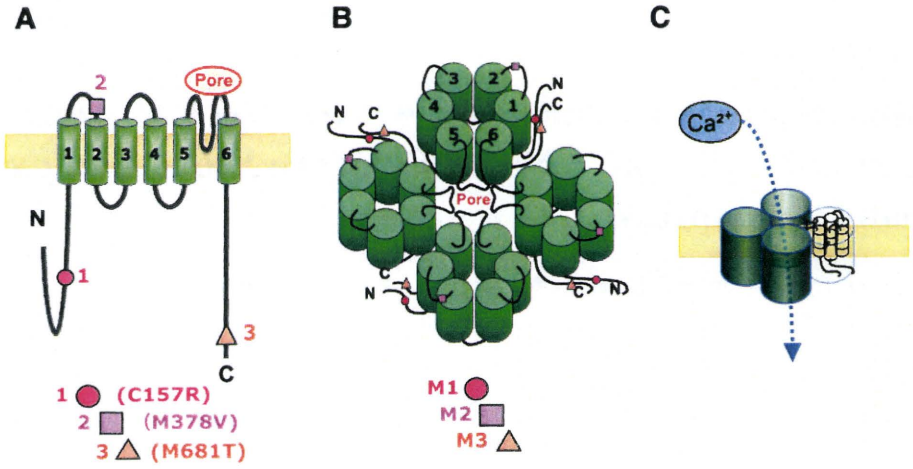

Fig. 1. Schema of ancestral- and derived (mutated)–TRPV6 channels. A: position of amino acid changes in ancestral- and derived (157C, 378M, 681M)–TRPV6 and their three-dimensional model (B). Pore: estimated pore-forming region in the TRPV6 channels. C: Extracellular Ca^{2+} enters into the pore in tetramized TRPV6 channels.

the sites of C157R, M378V, and M681T. In addition, these three SNPs have high posterior probabilities of being targets for directional selection (5, 6). These results suggest that the derived-TRPV6 is a strong candidate for positive selection in non-African populations. It is possible that such amino acid changes contribute to confer functional changes in the TRPV6 channels and it is likely that derived-TRPV6 having such an amino acid change might be beneficial for non-African populations.

The present study was thus designed to investigate functional differences between derived non-African TRPV6 and ancestral African TRPV6. To this end, we performed in vitro analysis to compare the capability of Ca^{2+} influx into the cells in derived-TRPV6 to that in the ancestral-TRPV6 with a set of experiments including electrophysiological assay, Ca^{2+}-imaging analyses, and morphological studies to detect efficacy of multimeric (possibly tetrameric) channel formation by visual fluorescence resonance energy transfer (FRET) analysis, recently performed in our laboratory (7 – 9). Our electrophysiological, Ca^{2+}-imaging, and FRET analyses using individual TRPV6 channel–expressing cells showed that it is likely that the derived-TRPV6 has the capability to absorb a much greater amount of Ca^{2+} from the intestine than the ancestral-TRPV6.

Materials and Methods

Drugs and chemicals

Gentamicin and sodium pyruvate were purchased from Sigma (St. Louis, MO, USA). Other chemicals used in the study were of analytical grade and obtained from Nacalai Tesque (Kyoto).

Construction of TRPV6 expression vectors

The complete coding region of the *TRPV6* gene was amplified from human placental cDNA (Clontech, Mountain View, CA) using the primers 5′-GCCGAATTC GAGACAGGAGACGGGACCTCTACA-3′ [an *Eco*RI recognition site (underlined) was introduced artificially] and 5′-GCCAAGCTTACCTCTGGGTGTTTGGTTTT TGTTT-3′ [a *Hin*dIII recognition site (underlined) was introduced artificially]. The amplification was performed in 25 μl of a mixture of 1 × buffer and 0.5 U of Phusion High-Fidelity DNA polymerase (New England BioLabs, Espoo, Finland). The temperature profile was denaturation at 98°C for 30 s, followed by 35 cycles of denaturation at 98°C for 7 s, annealing at 68°C for 30 s, and extension at 72°C for 75 s. The PCR product was digested with *Eco*RI and *Hin*dIII and then ligated into a pGEM-He-Juel vector. The sequence of the insert was confirmed by DNA sequencing using internal primers. DNA sequencing was performed with an ABI Prism 310 genetic analyzer (Applied Biosystems, Foster City, CA, USA). The vectors containing the ancestral-TRPV6 were constructed by use of a QuikChange Multi Site-Directed Mutagenesis Kit (Stratagene, La Jolla, CA, USA) using the derived-TRPV6 as the template. The temperature profile for mutagenesis was denaturation at 95°C for 1 min, followed by 30 cycles of denaturation at 95°C for 1 min, annealing at 55°C for 1 min, and extension at 65°C for 12 min. The mismatch primers used were MP157 (5′-TTCCGCCGTAGTCCCCGCAACCTCATCTA C-3′), MP378 (5′-TTCAGGAAGCCTACGTGACCCC TAAGGACG-3′), and MP681 (5′-CCTGTCCCTTCCT ACGCCCTCAGTGTCTCG-3′). The sequences of the mutants were verified by sequencing. For construction of the fluorescent protein–fused TRPV6, we used the brighter variant of the cyan fluorescent protein Cerulean (10), which was kindly donated by Dr. D.W. Piston (Vanderbilt University, Nashville, TN, USA) and the brighter variant of the yellow fluorescent protein Venus (11), which was generously given to us by Dr. T. Nagai (Hokkaido University, Hokkaido). The TRPV6-Cerulean

and TRPV6-Venus in each ancestral- and derived-TRPV6 were generated by ligating the channel cDNAs into Hind III sites into the corresponding sites of Cerulean and Venus cDNAs.

Construction of G-CaMP2-NT expression vector

To visualize intracellular Ca^{2+} concentration ($[Ca^{2+}]_i$) beneath the plasma membrane, we created a pN1-G-CaMP2-NT vector carrying the novel plasma membrane–targeted Ca^{2+}-sensor G-CaMP2-NT, in which a targeting signal for attachment to the plasma membrane (LCCMRRTKQVEKNDEDQKI, deduced amino-acid residues in single-letter codes) (12) was fused at the N-terminus end of G-CaMP2 (GenBank accession no. DQ381402) (13). The cDNA sequence for the targeting signal was amplified by PCR. The PCR primers, designed to anneal themselves, were as follows: 5′-GGAGATCTG GATCCGATATCCGCCACCATGCTGTGCTGTAT GAGAAGAACCAAACAGG-3′ and 5′-GGGTCGAC AATCTTTTGGTCCTCATCATTCTTTTCAACCTG TTTGGTTCTTCTCATACAGC-3′. The 0.09-kb PCR product was digested with *Bgl*II and *Sal*I and ligated with the 1.25-kb *Sal*I-*Not*I fragment from pN1-G-CaMP2 (13) and with the 3.94-kb *Bgl*II-*Not*I vector fragment from pN1-G-CaMP (14). The construct was verified by sequencing.

Oocyte preparation and cRNA injection

Immature V and VI oocytes from *Xenopus* were dissociated enzymatically as described previously (15). Isolated oocytes were incubated at 18°C in ND96 medium (96 mM NaCl, 2 mM KCl, 1.8 mM $CaCl_2$, 1 mM $MgCl_2$, and 5 mM HEPES, pH 7.4) containing 2.5 mM sodium pyruvate and 50 mg/ml gentamicin. For expression in *Xenopus* oocytes, all cDNAs for the synthesis of cRNAs were subcloned into the pGEM-He-Juel vector, which provided the 5′- and 3′-untranslated regions of the *Xenopus* β-globin RNA, ensuring a high level of protein expression in the oocytes (16). Each of the cRNAs was synthesized with a mCAP mRNA Capping Kit and with a T7 RNA polymerase in vitro Transcription Kit (Ambion, Austin, TX, USA) from the respective linearized cDNAs (7 – 9). For measurement of TRPV6-mediated currents induced by extracellular Ca^{2+}, cRNA for the ancestral- or derived-TRPV6 (each 5 ng) was injected into oocytes. The final injection volume was <50 nl in all cases. Oocytes were incubated in ND96 and used 3 – 8 days after injection as reported previously (15).

Electrophysiological recording with oocyte system

Electrophysiological recordings were performed using the two-electrode voltage clamp technique with a Geneclamp 500 amplifier (Axon Instruments, Foster City, CA, USA) at room temperature. Oocytes were clamped at −60 mV and continuously superfused with nominally Ca^{2+}-free ND96 buffer in a 0.25-ml chamber at a flow rate of 5 ml/min. Voltage recording microelectrodes were filled with 3 M KCl, and their tip resistance was 0.6 – 2.0 MΩ. Currents were continuously recorded and stored using MacLab (AD Instruments, Castle Hill, NSW, Australia) on a Macintosh computer, as described previously (7, 17).

Mammalian cell culture and transfection

Baby hamster kidney (BHK) cells or human embryonic kidney (HEK) 293T cells were grown in Dulbecco's modified Eagle's medium (DMEM) supplemented with 10% fetal bovine serum (FBS), penicillin (100 U/ml), and streptomycin (100 mg/ml) at 37°C in a humidified atmosphere of 95% air – 5% CO_2. BHK cells were used for fluorescent imaging studies, and HEK293T cells were used for the patch clamp study. BHK cells were seeded at a density of 1×10^5 cells per 35-mm glass-bottomed culture dish (Fluoro Physiotech, Tokyo) for 24 h. All cDNAs for transfection of mammalian cells were subcloned into pcDNA3.1(−) (Invitrogen, San Diego, CA, USA). Cells were used for analysis approximately 24 h after transfection. For patch clamp recordings of HEK293T cells, 0.2 μg of cDNAs for ancestral- or derived-TRPV6-Venus with 0.1 μg of G-CaMP2-NT was transfected. For Ca^{2+} imaging with BHK cells, 0.2 μg of each channel with 0.1 μg of G-CaMP2-NT cDNA was transfected. For Western blotting of HEK293T cells, 0.2 μg of ancestral- or derived-TRPV6 (see *Western blot analysis* section) was also transfected.

Electrophysiological recordings with HEK293T cells

For electrophysiological recordings, we basically followed the procedures of Bodding et al. (18, 19). Briefly, HEK293T cells on coverslips were transfected with one TRPV6-Venus, transferred to the recording chamber, and kept in a modified Ringer's solution (145 mM tetraethylammonium chloride, 10 mM $CaCl_2$, 10 mM CsCl, 2.8 mM KCl, 2 mM $MgCl_2$, 10 mM HEPES, adjusted to pH 7.2 with NaOH). Patch clamp experiments were conducted in the tight-seal whole cell configuration using an EPC-7 amplifier (HEKA, Tokyo). Recording microelectrodes were filled with the standard internal solution (145 mM cesium glutamate, mM HEPES, 8 mM NaCl, 1 mM $MgCl_2$, 2 mM MgATP, adjusted to pH 7.2 with CsOH) and their tip resistance was 2 to 3 MΩ. Currents were filtered using an 8-pole Bessel filter at 2.9 kHz. Cells for patch clamp experiments were identified by visualizing the Venus fluorescence with an inverted fluorescence microscope. Current–voltage (IV) relationships were measured by application of voltage-steps at a hold-

ing potential of −10 mV from −110 to 30 mV in 10-mV increment of 200-ms duration at 0.5 Hz using pClamp software (Axon Instruments). Currents were measured at the end of pulse during the last 40 ms of each pulse. Membrane potentials were corrected for 10-mV liquid junction potentials. All experiments were carried out at room temperature (20°C – 23°C); internal solutions were kept on ice to minimize ATP hydrolysis. The data were analyzed using Clampfit (Axon Instruments) and SigmaPlot (SPSS, Inc., Chicago, IL, USA).

Western blot analysis

Goat polyclonal TRPV6 antibody (N-16) and actin antibody were obtained from Santa Cruz Biotechnology (Santa Cruz, CA, USA). An anti-rabbit polyclonal GFP antibody that recognizes GFP as well as Cerulean and Venus was kindly provided by Dr. N. Saito of Kobe University (Kobe). *Xenopus* oocytes were injected with the ancestral- or derived-TRPV6 cRNA, and HEK293T cells were transfected with ancestral- or derived-TRPV6/TRPV6-Venus. For protein isolation, oocytes or HEK293T cells expressing each TRPV6 were sonicated and solubilized in PRO-PREP protein extraction buffer containing a combination of protease inhibitors (iNtRON Biotechnology, Sungnam, Korea) for 1 h at 4°C, as reported previously (8, 9). The mixtures were centrifuged (15,000 rpm, 30 min), and the supernatants were stored at −80°C until Western blot analysis. The supernatants were dissolved in Laemmli sample buffer containing 0.1 M dithiothreitol, subjected to 7.5% SDS-polyacrylamide gel electrophoresis (PAGE), transferred to polyvinylidene fluoride (PVDF) membranes, and subjected to immunoblotting using the polyclonal TRPV6 antibody (1:200). This was followed by a secondary goat anti-IgG conjugated with horseradish peroxidase (HRP) at 1:2,000 dilution for detection and then reacted with Western blot chemiluminescence detection reagents (Nacalai Tesque). In some experiments, the anti-rabbit GFP polyclonal antibody (1:10,000) was followed by a secondary rabbit anti-IgG with HRP (1:5,000) and the actin antibody (1:10,000) was followed by a secondary goat anti-IgG with HRP (1:10,000).

Ca^{2+} imaging of TRPV6-expressing BHK cells with the Ca^{2+}-sensor G-CaMP2-NT

Ca^{2+} imaging was performed using BHK cells coexpressing each of the TRPV6 with the Ca^{2+}-sensor G-CaMP2-NT, which localizes mostly just beneath the plasma membrane (13, 20). Cells placed in 35-mm glass-bottom dishes (1×10^5 cells/dish) were transfected with 0.2 μg of the ancestral- or derived-TRPV6 together with 0.1 μg G-CaMP2-NT. The fluorescence of G-CaMP2-NT was continuously recorded at a wavelength of 510 nm, and the fluorescence intensity in each whole cell was measured. Then, the extracellular medium was changed from a nominally Ca^{2+}-free buffer to a buffer containing 18 mM Ca^{2+}. Data were calculated with the LSM510 META software (Carl Zeiss, Jena, Germany) and expressed as intensity of fluorescence (510 nm) and compared with fluorescence intensity of the cells in the nominally Ca^{2+}-free medium.

FRET analysis by confocal microscopy

Protein complex formation of TRPV6-Cerulean and TRPV6-Venus was analyzed using FRET capability of the confocal microscope. BHK cells cultured in 35-mm glass-bottomed dishes were cotransfected with 0.2 μg of Cerulean- or Venus-tagged ancestral-TRPV6 and/or derived-TRPV6. A 63× magnification, 1.25-aperture oil immersion objective was used with a pinhole for visualization. Cerulean and Venus were both excited by a 458-nm laser, and images of live cells were taken by placing the dish onto the stage of the confocal microscope LSM510 META, as described previously (7 – 9).

Photobleaching and calculation of FRET efficiency

To confirm FRET between Cerulean and Venus, we monitored FRET-acceptor photobleaching in BHK cells coexpressing TRPV6-Venus and TRPV6-Cerulean, as reported previously (7 – 9). In brief, FRET was measured by imaging Cerulean before and after photobleaching Venus with a 514-nm argon laser at 100% power intensity. As a control, we examined the FRET efficiency of at least three areas of unbleached membranes in the same cell. FRET efficiency was then calculated using the equation $E = (I_D - I_{DA}) / I_D$, where I_{DA} is the peak of donor (Cerulean) emission in the presence of the acceptor and I_D is the peak in the presence of the sensitized acceptor, as described previously (7 – 9, 21).

Statistical analysis of functional analyses

Data are expressed as means ± S.E.M. Differences between two groups were examined for statistical significance using Student's *t*-test. Prism software (GraphPad Software, La Jolla, CA, USA) was used to analyze data for statistical significance and to analyze data and fit curves for extracellular Ca^{2+} dose–responses. A *P* value less than 0.05 denoted the presence of a statistically significant difference.

Results

Effect of three nonsynonymous SNPs in TRPV6 channels on the properties of Ca^{2+} influx

Xenopus oocytes are a useful system for functional electrophysiological analysis of ion channels and Ca^{2+}-

mobilizing G protein–coupled receptors (15, 22) and also have been used for an analysis of TRPV6-channel function by detecting Ca^{2+}-activated Cl^--channel activity endogenously expressed in oocytes (23). When TRPV6 is activated by addition of extracellular Ca^{2+}, increases in $[Ca^{2+}]_i$ stimulate Ca^{2+}-activated Cl^- channels to elicit robust Cl^- currents (23), suggesting that the amplitude of the Cl^- currents reflected the increases in $[Ca^{2+}]_i$ resulting from TRPV6-mediated Ca^{2+} influx. In oocytes expressing ancestral-TRPV6, a change from the nominally Ca^{2+}-free buffer to the 1.8 mM Ca^{2+}–containing ND96 buffer elicited dual phase inward currents (Fig. 2A), as reported previously in oocytes expressing TRPV6 (23) and oocytes directly injected with $CaCl_2$ beneath the plasma membrane (24). We confirmed that the currents elicited by addition of Ca^{2+} were composed of outward Cl^- currents through activation of the Ca^{2+}-activated Cl^- channels, based on the current–voltage relationship curve as shown by other investigators (23) and our previous study (15). In oocytes expressing the derived-TRPV6, switching to the 1.8 mM Ca^{2+}–containing buffer induced much robust Cl^- currents compared with the oocytes expressing the ancestral-TRPV6 (Fig. 2: A and B). In oocytes injected with H_2O instead of TRPV6 cRNAs, no apparent currents were observed (Fig. 2: A and B). When varying concentrations of extracellular Ca^{2+} (0.2, 0.4, 0.9, 1.8, and 9 mM) were applied, derived-TRPV6 showed higher Ca^{2+}-influx activity than ancestral-TRPV6 in all the concentrations used (Fig. 2C). Western blot analysis using actin antibody as the internal standard showed that both groups of oocytes expressed almost the same amount of proteins (Fig. 2D). Band intensities obtained with TRPV6 antibody showed that both channels were similarly expressed in the oocytes (Fig. 2D).

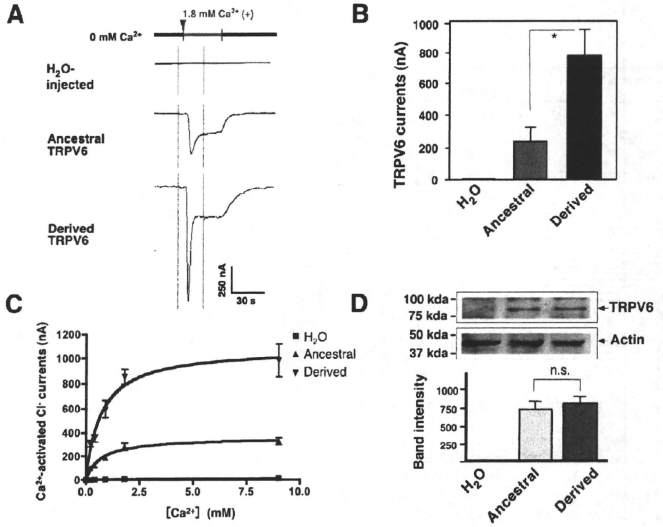

Fig. 2. Effects of addition of extracellular Ca^{2+} on the activity of Ca^{2+}-activated Cl^- channels in *Xenopus* oocytes expressing ancestral- or derived-TRPV6. A: Typical tracings of Ca^{2+}-activated Cl^- currents by addition of ND96 buffer containing 1.8 mM $CaCl_2$ in oocytes with or without expressing ancestral- or derived-TRPV6 at holding potential of −60 mV. B: Ancestral- or derived-TRPV6–mediated Ca^{2+}-activated Cl^- currents. Data are the mean ± S.E.M. values from 10 each oocytes. Ancestral: ancestral-TRPV6, Derived: derived-TRPV6. Significantly different ($*P < 0.05$) from the mean of the ancestral TRPV6. C: Concentration-dependent activation of Ca^{2+}-activated Cl^- currents in oocytes expressing ancestral- or derived-TRPV6. Note that oocytes expressing derived TRPV6 show superior Cl^- currents in all Ca^{2+} concentration used. D: Western blot analysis of the TRPV6 proteins extracted from oocytes. H_2O: oocytes injected with H_2O, Ancestral: oocytes injected with ancestral-TRPV6, Derived: oocytes injected with derived-TRPV6. Top: bands detected with TRPV6 antibody (83 kda). Middle: bands detected with actin antibody (42 kda) with the same Western-blot membranes. Bottom: summary of the band intensity with TRPV6 antibody. Not significant (n.s) band intensity was detected with TRPV6 antibody between oocytes expressing ancestral- or derived-TRPV6.

The differences between Ca^{2+}-activated Cl^- currents observed in oocytes expressing ancestral- and derived-TRPV6 are assumed to be due to different amounts of Ca^{2+} influx through the individual TRPV6. To further directly compare the functional differences between ancestral- and derived-TRPV6, we performed patch clamp analysis with HEK293T cells transfected with the fluorescent protein Venus–tagged ancestral- or derived-TRPV6. To confirm whether TRPV6-Venus and non-tagged TRPV6 have similar properties, we injected cRNAs encoding ancestral-TRPV6-Venus or derived-TRPV6-Venus into oocytes. In the electrophysiological experiments, we found that both tagged-TRPV6 elicited Ca^{2+}-activated Cl^- current similar to those of non-tagged ancestral- or derived-TRPV6 (ancestral type, TRPV6 248.2 ± 32 nA, TRPV6-Venus 278.0 ± 29 nA; derived type, TRPV6 740.6 ± 90.3 nA, TRPV6-Venus 820.8 ± 85.0 nA, n = 10 each) at holding potential of −60 mV.

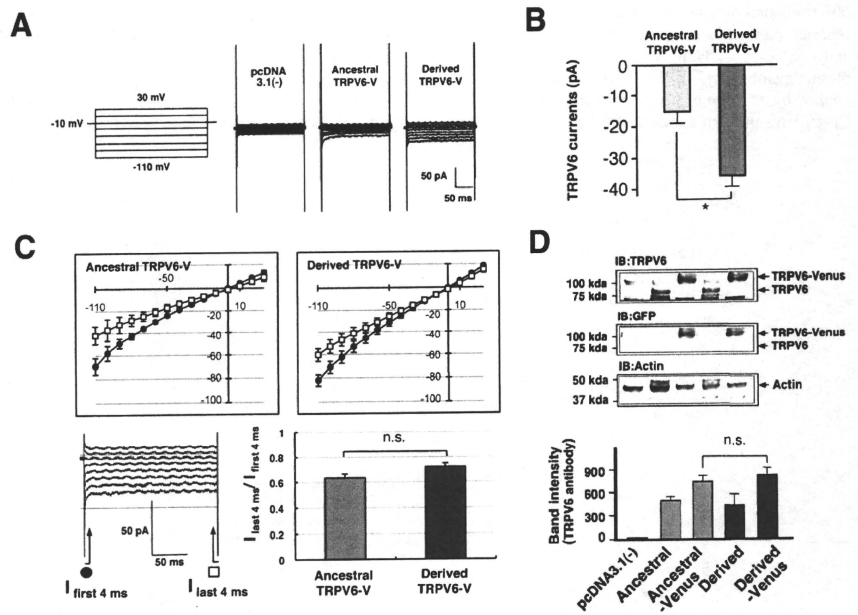

Fig. 3. Current–voltage relationship of the Ca^{2+}-induced inward current I_{TRPV6} in HEK293T cells transfected with the pcDNA3.1(−) vector alone, ancestral-, or derived-TRPV6-Venus (TRPV6-V). A: Left, voltage step command. Currents were evoked by voltage steps between −110 to 30 mV (200-ms duration) with the holding potential of −10 mV. Right, representative currents evoked by the voltage steps after maximum activation of the inward currents by 10 mM Ca^{2+} in pcDNA3.1(−) vector–, ancestral-TRPV6-Venus–, or derived-TRPV6-Venus–expressing cells. B: Extracellular Ca^{2+}-induced inward currents through ancestral- or derived-TRPV6-V after subtraction of control currents obtained from cells expressing pcDNA3.1(−) alone. Data are the mean ± S.E.M. values (n = 17, ancestral-TRPV6-V; n = 21, derived-TRPV6-V). Significantly different (*$P < 0.05$) from the mean of the ancestral-TRPV6-V. C: Current–voltage relationships (IV curves) for the ancestral- or derived forms of TRPV6-V measured from 4-ms average at the start (4 ms after the beginning of the voltage step, $I_{first\ 4\ ms}$) and the end of the pulse (4 ms prior to the end of the voltage step, $I_{last\ 4\ ms}$) as indicated by the arrows (n = 8 for each group of the cells). The voltage-step protocol was the same as in panel A. Summary of the ratio of $I_{last\ 4\ ms}/I_{first\ 4\ ms}$ (Right bottom panel C). n.s.: No significant difference of $I_{last\ 4\ ms}/I_{first\ 4\ ms}$ ratio between cells expressing ancestral- and derived-TRPV6-V. D: Western blot analysis of the TRPV6 proteins extracted from HEK293T cells. Top, immunoblotted with antibody against TRPV6. Middle, immunoblotted with antibody against GFP. TRPV6-V (110 kda), TRPV6 (83 kda). Bottom, immunoblotted with antibody against actin, and summarized data of band intensities immunoblotted with TRPV6 antibody (n = 4). n.s.: No significant difference between band intensities with cells expressing ancestral- and derived-TRPV6-V.

In control HEK293T cells transfected with pcDNA3.1(−) vector alone, inward currents (−37.17 ± 6.83 pA, n = 13) were observed to the switch holding potential from −10 to −110 mM. This is probably due to endogenously expressed Ca^{2+}-permeable TRPV channels (possibly TRPV5 and/or TRPV6) in HEK293T cells. In the cells transfected with ancestral-TRPV6-Venus, a robust increment in the Ca^{2+}-induced inward current was observed (−51.37 ± 3.25 pA, n = 17) (Fig. 3: A and B) similarly as previously reported (18, 19). Further increases in Ca^{2+}-induced inward currents were observed in cells transfected with derived-TRPV6-Venus (−70.0 ± 2.64 pA, n = 21) (Fig. 3: A and B). I–V relationship analysis showed an inward rectification profile, and a fast initial decay was observed in both ancestral-TRPV6-Venus– and derived-TRPV6-Venus–expressing cells, particularly at the negative voltage of <−40 mV (Fig. 3C, Top panel). This decrease in Ca^{2+} entry from the first 4-ms currents after beginning of the voltage-steps to the end of 4-ms currents during the 200-ms voltage-step at −110 mV is based on channel inactivation induced by increase in $[Ca^{2+}]_i$ (18, 19). TRPV6 channels are characterized by their Ca^{2+}-induced inactivation during hyperpolarizing voltage steps, and this Ca^{2+}-dependent feedback inhibition affects the properties of TRPV6 channels (3, 18, 19). We thus compared the efficacy of the Ca^{2+}-

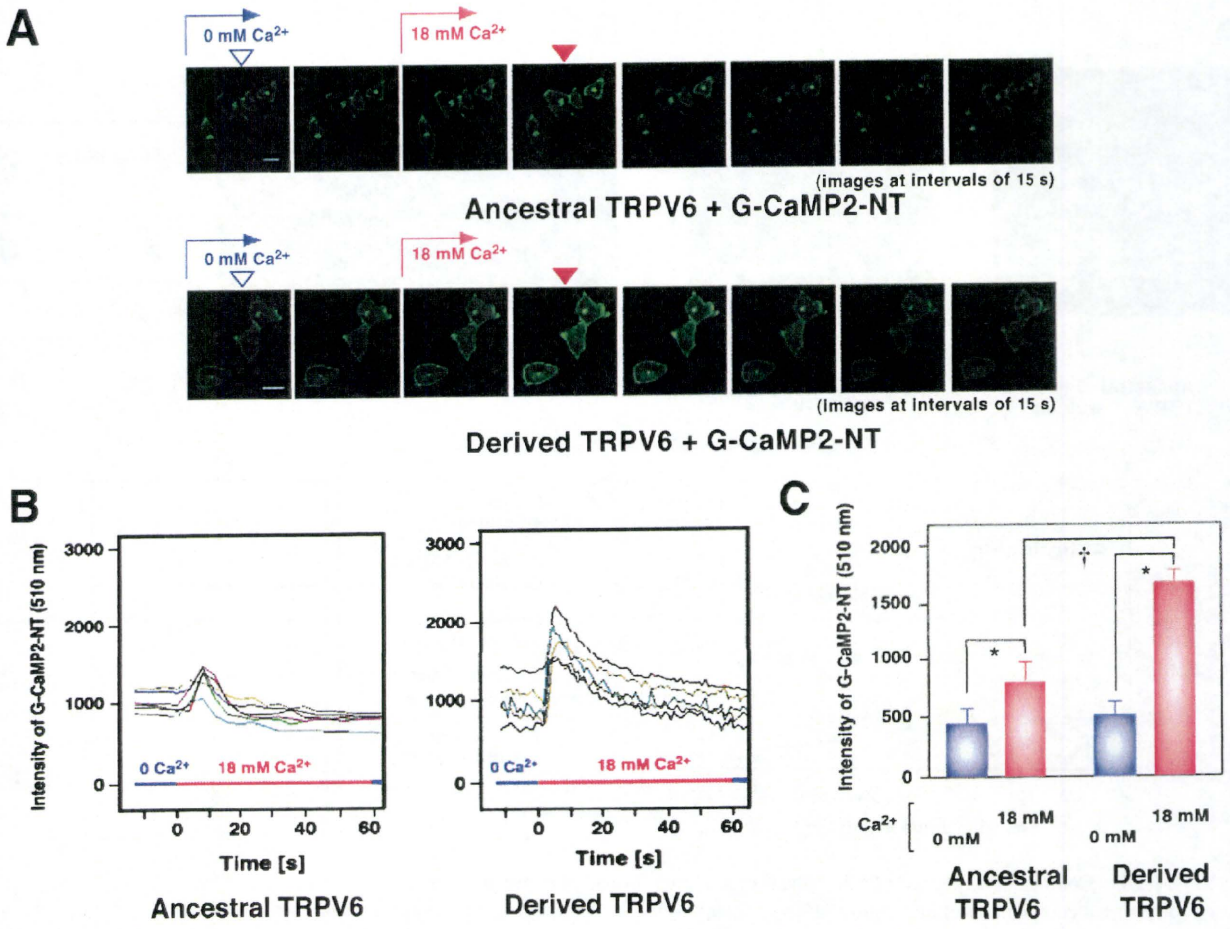

Fig. 4. Ca^{2+} imaging of BHK cells coexpressing individual TRPV6 together with the Ca^{2+}-sensor protein G-CaMP2-NT. A: Time course of visualized G-CaMP2-NT intensity following addition of 18 mM $CaCl_2$ to the buffer of BHK cells coexpressing ancestral-TRPV6 (Top) or derived-TRPV6 (Bottom). Calibration bar = 10 μm. B: Time course of intensity of G-CaMP2-NT fluorescence (510 nm) in cells transfected with ancestral-TRPV6 (Left) or derived-TRPV6 (Right) together with G-CaMP2-NT. The transfected cells were stimulated with 18 mM extracellular Ca^{2+} for 60 s. Note that similar steep increases and decay of fluorescence intensity were observed. G-CaMP2-NT intensity was measured at individual whole cell area with the Carl Zeiss Meta software. C: Intensity of G-CaMP2-NT fluorescence (510 nm) in BHK cells expressing ancestral- or derived-TRPV6. Fluorescence intensities were measured as in panel B before (open arrowhead) and after (closed arrowhead) the addition of Ca^{2+} in panel A. Data are the mean ± S.E.M. values of 6 independent experiments (n = 36 – 40). Significantly different ($^*P < 0.05$) from the intensity without Ca^{2+} and significantly different ($^\dagger P < 0.05$) from the intensity in cells expressing ancestral-TRPV6.

inactivation profiles between cells expressing ancestral- and derived TRPV6-Venus. As shown in the right bottom panel of Fig. 3C, the ratio of the currents ($I_{last\ 4\ ms}/I_{first\ 4\ ms}$) at the voltage step of −110 mV was not significantly different, suggesting that there were no differences in the Ca^{2+}-inactivation processes between the ancestral- and derived-TRPV6 channels. Western blot analysis using TRPV6 antibody and the GFP antibody that can detect Venus protein showed that each group of cells expressed almost the same amount of individual TRPV6-Venus or TRPV6 transfected with ancestral-TRPV6, ancestral-TRPV6-Venus, derived-TRPV6, or derived-TRPV6-Venus cDNAs (Fig. 3D). With the same membranes we confirmed that almost same amounts of proteins were eluted in each lane by detecting actin protein as an internal standard (Fig. 3D).

We further sought to examine increases in $[Ca^{2+}]_i$ induced by activation of ancestral- or derived-TRPV6 channels. In BHK cells coexpressing ancestral-TRPV6 together with G-CaMP2-NT, which allows visualization of changes in $[Ca^{2+}]_i$ beneath the plasma membrane (14, 20 and see Materials and Methods), addition of 18 mM Ca^{2+} increased the intensity of green fluorescence beneath the plasma membrane and the cytosol (Fig. 4A). In cells expressing the derived-TRPV6 instead of the ancestral-TRPV6, a much brighter green fluorescence was observed

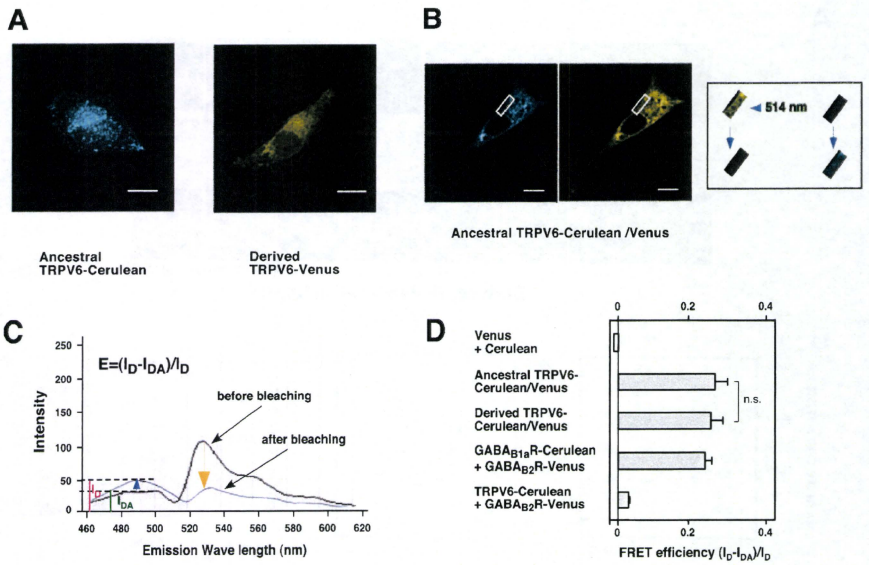

Fig. 5. Confocal imaging and FRET analysis of multimer formation between ancestral- and derived-TRPV6 in BHK cells coexpressing a combination of ancestral-TRPV6-Cerulean/Venus or derived-TRPV6-Cerulean/Venus. A: Visualization of ancestral-TRPV6-Cerulean and derived-TRPV6-Venus at the plasma membrane and cytosol in BHK cells. Similar fluorescence was observed in cells expressing ancestral-TRPV6-Venus or derived-TRPV6-Cerulean (data not shown). Calibration bar = 10 μm. B: Changes in fluorescence induced by acceptor photobleaching (15-s application at 514 nm) in BHK cells coexpressing ancestral-TRPV6-Cerulean/Venus. C: Emission spectra from a BHK cell before and after Venus photobleaching as indicated in panel B. Note the increase of the Cerulean peak emission (488 nm) following photobleaching of Venus (528 nm). The mathematical equation used for calculating the FRET efficiency (E) is also shown. I_{DA}, peak of donor emission in the presence of acceptor; I_D, peak of donor emission in the presence of sensitized acceptor. D: Comparison of FRET efficiency for ancestral-TRPV6-Cerulean/Venus and derived-TRPV6-Cerulean/Venus. The combination of Venus + Cerulean and $GABA_{B1a}$R-Cerulean + $GABA_{B2}$R-Venus pairs was used as negative and positive controls for protein–protein interaction, respectively. Each bar represents the mean ± S.E.M. of FRET efficiency in independent experiments using three regions of interest per BHK cell in six cells (n = 18). n.s.: No significant difference of FRET efficiency between ancestral-TRPV6-Cerulean/Venus and derived-TRPV6-Cerulean/Venus.

(Fig. 4: A – C), demonstrating that the derived-TRPV6 transported larger amounts of Ca^{2+} into the cells than the ancestral one. The time course of $[Ca^{2+}]_i$ shown in Fig. 4B demonstrated that steep increases and fast inactivation of $[Ca^{2+}]_i$ were observed in both of the TRPV6 channels, which were typical properties of TRPV6 channels.

FRET analysis after acceptor photobleaching in BHK cells coexpressing ancestral- or derived-TRPV6

TRPV6 is considered to form homotetramers by itself or heterotetramers with TRPV5 (25). Using FRET measurement after acceptor photobleaching techniques, previously performed in our laboratories (7 – 9), we investigated whether the ancestral-TRPV6 and derived-TRPV6 form multimers (possibly tetramers). Fluorescence from the ancestral-TRPV6-Cerulean and derived-TRPV6-Venus was diffuse in the cells (Fig. 5A). The ancestral-TRPV6-Venus and derived-TRPV6-Cerulean fluorescence were also similarly diffuse in the cells, (data not shown). Acceptor photobleaching analysis of BHK cells coexpressing the ancestral-TRPV6-Cerulean/Venus showed a decrease in Venus intensity associated with an increase in Cerulean fluorescence (Fig. 5: B and C), indicating formation of a protein complex between the ancestral-TRPV6-Cerulean/Venus molecules, as shown in our previous studies (7 – 9). The FRET efficiency of the ancestral-TRPV6-Cerulean/Venus and that of the derived-TRPV6-Cerulean/Venus were similar (Fig. 5D), suggesting similar properties of multimer formation in both the ancestral- and derived-TRPV6. As a positive control, we measured FRET efficiency of the formation of functional $GABA_B$ receptors ($GABA_BR$) composed of $GABA_{B1a}R$ and $GABA_{B2}R$, which are known to form a heterodimer (7, 8). In contrast, almost no FRET was observed (Fig. 5D) in cells coexpressing Cerulean + Venus or the ancestral-TRPV6-Cerulean + $GABA_{B2}R$-Venus, indicating specific multimer formation of TRPV6 channels.

Discussion

In the TRPV6 gene, a pattern of positive selection was observed in a 115-kb region of chromosome 7q34-35 (4 – 6). *TRPV6* has three derived nonsynonymous SNPs (157C, 378M, 681M), which were in almost complete linkage disequilibrium and nearly fixed in non-African populations (Fig. 1) (4, 6). These three SNPs have high posterior probabilities of being targets for directional selection (5, 6), suggesting that the derived-TRPV6 having three SNPs is a strong candidate for positive selection in non-African populations. Changes in such amino acids might have contributed to confer functional changes in the TRPV6 channels, and it is likely that derived-TRPV6 having such an amino acid change would be beneficial for non-African populations.

The present study showed by several different functional methods that the capability for Ca^{2+}-influx increase in the derived-TRPV6 is greater than that of the ancestral-TRPV6 (Figs. 2 – 4). Oocytes expressing derived-TRPV6 showed much more robust Ca^{2+}-activated Cl^- currents in response to Ca^{2+} addition than those expressing ancestral-TRPV6, even though the protein expression levels of both channels were almost the same. Patch-clamp analysis also demonstrated that HEK293T cells expressing derived-TRPV6 but not ancestral-TRPV6 elicited much more Ca^{2+} influx, although both channel proteins were expressed equally. Furthermore, Ca^{2+}-imaging analysis demonstrated that extracellular Ca^{2+}-induced $[Ca^{2+}]_i$ increase was higher in cells expressing derived-TRPV6 than those expressing the ancestral one. In addition, Ca^{2+}-dependent feedback inhibition as demonstrated by Ca^{2+}-induced TRPV6 inactivation did not differ between ancestral- and derived-TRPV6. Finally, properties and efficiency of TRPV6-channel assembly to multimer channels were not significantly different between derived- and ancestral-TRPV6. Collectively these results indicate that the derived-TRPV6 itself has a greater capability to increase Ca^{2+} influx than ancestral-TRPV6.

On the other hand, Suzuki et al. (26) reported results different from our functional analysis data on ancestral- and derived-TRPV6; they showed that the ancestral-TRPV6 was more Ca^{2+}-permeable than the derived one with the $^{45}Ca^{2+}$-uptake assay using the *Xenopus* oocyte expression system. The reason for this discrepancy is unclear at present, but possible reasons for this difference are the different experimental design and extracellular Ca^{2+} concentration they used; they measured $^{45}Ca^{2+}$ influx to the oocytes at a single extracellular Ca^{2+} concentration (0.2 mM) as a functional TRPV6 assay. According to their report, the ancestral-TRPV6 may have higher Ca^{2+}-uptake properties at low Ca^{2+} concentration. However, this is unlikely because our results using different (0.2 – 9 mM) concentrations of extracellular Ca^{2+} showed that derived-TRPV6 elicited higher Ca^{2+}-influx activity (measured by Ca^{2+}-activated Cl^- currents) at all the tested concentrations, including 0.2 mM Ca^{2+}. We performed functional comparison of derived- and ancestral-TRPV6 with a combination of assay methods, but it will be necessary, nonetheless, to make detailed functional analyses of ancestral- and derived-TRPV6 to better understand the driving forces behind their functional differences.

As TRPV6 channels are involved in the rate-limiting step of dietary calcium absorption (1, 2), it seems that individuals having the derived-TRPV6 could absorb more dietary calcium from the intestine than individuals

having the ancestral one. It is well known that TRPV6 expression levels are associated with the activity of vitamin D_3, which requires ultraviolet light for its activation (1, 2). These findings may have implications for adaptation to calcium deficiency due to vitamin D_3 insufficiency, conferring an advantage to individuals with derived-TRPPV6 over individuals with the ancestral-TRPV6, especially in areas at high latitudes with low ultraviolet light exposure. This observation may provide a plausible explanation for the selective force for an increased frequency of the derived-TRPV6 with three nonsynonymous SNPs outside Africa.

Another possible explanation for the different Ca^{2+}-influx property between ancestral- and derived-TRPV6 is that some type of genetic event that impacted calcium homeostasis might have occurred in non-African populations but not in African populations. This explanation assumes that the importance of calcium uptake differs between the African and non-African populations. As speculated by Akey et al. (5), the presence of two different types of TRPV6 channels might be beneficial, and some form of balancing selection may have been acting on this locus in Africa (5). Indeed, a recent study suggests that the calcium ion is integral to proper immune function, and TRPV6 has been implicated as one of the modulators of T-cell activation (27). We speculate that if the signature of gene selection may have been related to pathogen susceptibility, individuals carrying the derived-TRPV6 channels in the non-African area may have resistance against some types of pathogens, while individuals carrying the ancestral-TRPV6 in Africa area may have resistance against other types of pathogens. Interestingly, a recent report showed that the A563T variation of renal epithelial TRPV5, channels that reabsorb Ca^{2+} into renal tubules, was expressed among African Americans, and this variant elicited enhanced Ca^{2+} influx by affecting the Ca^{2+}-permeation pathway compared with its wild type (28). They speculate that the A563T variant may contribute to the superior ability of renal Ca^{2+} conservation in African Americans (28).

SNPs in derived-TRPV6 were in almost complete linkage disequilibrium and almost no populations of TRPV6 with one or two positions of SNP (5), and it is not known at present which mutation(s) in the three derived-TRPV6 is/are important for their higher ability to permeate Ca^{2+}. Such experiments using site-directed derived-TRPV6 with only one changed amino acid (TRPV6-157C, TRPV6-378M, TRPV6-681M) are ongoing studies in our laboratory.

In conclusion, we showed that derived-TRPV6 is capable of increasing TRPV6-mediated Ca^{2+} influx, suggesting that individuals having the derived-TRPV6 could absorb more dietary calcium from the intestine than those having the ancestral-TRPV6, which provide a possible selective advantage, promoting the spread of the advantageous haplotype outside Africa, including the European area.

Acknowledgments

This work was supported by Grants-in-Aid for Scientific Research from the Ministry of Education, Culture, Sports, Science, and Technology of Japan (Y.U.); a grant from Daiichi Sankyo Pharmaceutical Co., Ltd. (Y.U.); Smoking Research Foundation (Y.U. and Y.S.); and a grant from Nagasaki University, Graduate School of Biomedical Sciences (Y.S.).

References

1 van Abel M, Hoenderop JG, Bindels RJ. The epithelial calcium channels TRPV5 and TRPV6: regulation and implications for disease. Naunyn Schmiedebergs Arch Pharmacol. 2005;371: 295–306.
2 Nijenhuis T, Hoenderop JG, Bindels RJ. TRPV5 and TRPV6 in Ca(2+) (re)absorption: regulating Ca(2+) entry at the gate. Pflugers Arch. 2005;451:181–192.
3 Venkatachalam K, Montell C. TRP channels. Annu Rev Biochem. 2007;76:387–417.
4 Akey JM, Eberle MA, Rieder MJ, Carlson CS, Shriver MD, Nickerson DA, et al. Population history and natural selection shape patterns of genetic variation in 132 genes. PLoS Biology. 2004;2:e286.
5 Akey JM, Swanson WJ, Madeoy J, Eberle M, Shriver MD. TRPV6 exhibits unusual patterns of polymorphism and divergence in worldwide populations. Hum Mol Genet. 2006;15: 2106–2113.
6 Stajich JE, Hahn MW. Disentangling the effects of demography and selection in human history. Mol Biol Evol. 2005;22:63–73.
7 Uezono Y, Kanaide M, Kaibara M, Barzilai R, Dascal N, Sumikawa K, et al. Coupling of GABAB receptor GABAB2 subunit to G proteins: evidence from Xenopus oocyte and baby hamster kidney cell expression system. Am J Physiol Cell Physiol. 2006;290:C200–C207.
8 Kanaide M, Uezono Y, Matsumoto M, Hojo M, Ando Y, Sudo Y, et al. Desensitization of GABA(B) receptor signaling by formation of protein complexes of GABA(B2) subunit with GRK4 or GRK5. J Cell Physiol. 2007;210:237–245.
9 Hojo M, Sudo Y, Ando Y, Minami K, Takada M, Matsubara T, et al. μ-Opioid receptor forms a functional heterodimer with cannabinoid CB_1 receptor: electrophysiological and FRET annsay analysis. J Pharmacol Sci. 2008;108:308–319.
10 Rizzo MA, Springer GH, Granada B, Piston DW. An improved cyan fluorescent protein variant useful for FRET. Nat Biotechnol. 2004;22:445–449.
11 Nagai T, Ibata K, Park ES, Kubota M, Mikoshiba K, Miyawaki A. A variant of yellow fluorescent protein with fast and efficient maturation for cell-biological applications. Nat Biotechnol. 2002; 20:87–90.
12 Zacharias DA, Violin JD, Newton AC, Tsien RY. Partitioning of lipid-modified monomeric GFPs into membrane microdomains of live cells. Science. 2002;296:913–916.
13 Lee MY, Song H, Nakai J, Ohkura M, Kotlikoff MI, Kinsey SP,

et al. Local subplasma membrane Ca^{2+} signals detected by a tethered Ca^{2+} sensor. Proc Natl Acad Sci U S A. 2006;103:13232–13237.

14 Nakai J, Ohkura M, Imoto K. A high signal-to-noise Ca(2+) probe composed of a single green fluorescent protein. Nat Biotechnol. 2001;19:137–141.

15 Uezono Y, Bradley J, Min C, McCarty NA, Quick M, Riordan JR, et al. Receptors that couple to 2 classes of G proteins increase cAMP and activate CFTR expressed in Xenopus oocytes. Receptors Channels. 1993;1:233–241.

16 Ivanina T, Varon D, Peleg S, Rishal I, Porozov Y, Dessauer CW, et al. Galphai1 and Galphai3 differentially interact with, and regulate, the G protein-activated K+ channel. J Biol Chem. 2004; 279:17260–17268.

17 Uezono Y, Akihara M, Kaibara M, Kawano C, Shibuya I, Ueda Y, et al. Activation of inwardly rectifying K+ channels by GABA-B receptors expressed in *Xenopus* oocytes. Neuroreport. 1998;9: 583–587.

18 Bodding M, Wissenbach U, Flockerzi V. The recombinant human TRPV6 channel functions as Ca^{2+} sensor in human embryonic kidney and rat basophilic leukemia cells. J Biol. Chem. 2002;277: 36656–36664.

19 Bodding M, Fecher-Trost C, Flockerzi V. Store-operated Ca^{2+} current and TRPV6 channels in lymph node postate cancer cells. J Biol Chem. 2003;278:50872–50879.

20 Tallini YN, Ohkura M, Choi BR, Ji G, Imoto K, Doran R, et al. Imaging cellular signals in the heart in vivo: cardiac expression of the high-signal Ca^{2+} indicator GCaMP2. Proc Natl Acad Sci U S A. 2006;103:4753–4758.

21 Riven I, Kalmanzon E, Segev L, Reuveny E. Conformational rearrangements associated with the gating of the G protein-coupled potassium channel revealed by FRET microscopy. Neuron. 2003; 38:225–235.

22 Dascal N. The use of *Xenopus* oocytes for the study of ion channels. CRC Crit Rev Biochem. 1987;22:317–387.

23 Peng JB, Chen XZ, Berger UV, Vassilev PM, Brown EM, Hediger MA. A rat kidney-specific calcium transporter in the distal nephron. J Biol Chem. 2000;275:28186–28194.

24 Miledi R, Parker I. Chloride current induced by injection of calcium into Xenopus oocytes. J Physiol. 1984;357:173–183.

25 Hoenderop JG, Voets T, Hoefs S, Weidema F, Prenen J, Nilius B, et al. Homo- and heterotetrameric architecture of the epithelial Ca^{2+} channels TRPV5 and TRPV6. Embo J. 2003;22:776–785.

26 Suzuki Y, Pasch A, Bonny O, Mohaupt MG, Hediger MA, Frey FJ. Gain of function haplotype in the epithelial calcium channel TRPV6 is a risk factor for renal calcium stone formation. Hum Mol Genet. 2008;17:1613–1618.

27 Cui J, Bian JS, Kagan A, McDonald TV. CaT1 contributes to the stores-operated calcium current in Jurkat T-lymphocytes. J Biol Chem. 2002;277:47175–47183.

28 Na T, Zhang W, Jiang Y, Liang Y, Ma HP, Warnock DG, et al. The A563T variation of the renal epithelial calcium channel TRPV5 among African Americans enhances calcium influx. Am J Physiol Renal Physiol. 2009;296:F1042–F1051.

鎮痛薬による臓器障害

鈴木雅美　上園保仁
国立がん研究センター研究所がん患者病態生理研究部

要　旨
鎮痛薬が引き起こす副作用は多岐にわたり，時には生命を脅かす臓器障害をもたらすこともある．いわゆる“痛み止めの薬”として頻用されている非ステロイド性鎮痛薬（NSAIDs）は，胃腸，腎，心血管系などのほとんどの臓器に毒性を示す可能性がある．一方，アセトアミノフェンは，大量投与により肝障害を引き起こすが，適切に用いれば有害作用を生じることは少ない．鎮痛補助薬であるカルバマゼピンは，骨髄抑制を引き起こすため，抗がん剤を使用しているがん性疼痛患者では，汎血球減少症のリスクが高まる．ステロイドは短期投与では安全域の広い薬物であるが，長期投与では骨粗鬆症や感染症，胃腸障害が出現する．本稿では，臨床で比較的頻繁に認められる鎮痛薬による臓器障害について概説する．
（ペインクリニック 31：1177-1183，2010）
キーワード：鎮痛薬，臓器障害，リスクファクター

はじめに

痛みの病態生理に基づいた各種鎮痛薬の選択により，薬物療法の有効性が飛躍的に高まることが期待されている．一方，鎮痛薬が引き起こす副作用は多岐にわたり，時には生命を脅かす臓器障害をもたらすこともある．高齢者やがん性疼痛患者は，多くの疾病を併発していることに加え，多種類の薬物を服用していることから，重篤な副作用が出現しやすい．臨床的に重要なことは，薬物が起こしうる臓器障害とそのハイリスクファクターを常に念頭におき，注意深く対処することである．

本稿では，臨床において比較的頻繁に認められる鎮痛薬ならびに鎮痛補助薬による臓器障害に焦点をあて，その薬物の鎮痛作用発現機序と臓器障害の発現について紹介する．

1．非ステロイド性鎮痛薬（Nonsteroidal anti-inflammatory drugs：NSAIDs）

NSAIDsは，主に軟部組織の損傷，筋挫傷，捻挫，頭痛および関節炎などの軽度から中等度の痛みに対して有効な薬物である．がん性疼痛では，WHO方式三段階除痛ラダーの第一段階から第三段階のどの時期においても幅広く使用され，オピオイド鎮痛薬との併用により相乗効果を発揮することから，オピオイド鎮痛薬の用量の節減においても有用性が高い．

NSAIDsの鎮痛作用の発現機序は，シクロオキシゲナーゼ（cyclooxygenase：COX）の活性化を阻害することによるプロスタグランジン（prostaglandin：PG）類合成抑制である[1]．COXはCOX-1とCOX-2の2つのサブタイプが知られている．COX-1は胃粘膜，腎，血小板などほとんどの正常組織に存在する常在型の

〈Review〉
Analgesic agent : Overview of the organ damage
Masami Suzuki, Yasuhito Uezono
Cancer Pathophysiology Division, National Cancer Center Research Institute

酵素であり，PG産生により胃粘膜保護，腎血流の維持，血管拡張などの生理作用を担っている．一方，COX-2は炎症性サイトカインにより，マクロファージや血管内皮細胞などの炎症関連細胞に発現する誘導型の酵素である[1]．炎症部において産生されたPGE_2およびPGI_2は，侵害受容性神経線維終末のPG受容体に結合し，神経線維の興奮性を高め，ブラジキニンやヒスタミンなどの発痛・起炎物質による痛み反応を増強させる．したがってNSAIDsは，主に末梢の炎症局所におけるPG作用を抑制することで鎮痛作用を発現する．また近年，病態下においてNSAIDsは，末梢のみならず中枢神経系に作用し，鎮痛効果を発現することが明らかにされている[2]．

1）NSAIDsによる胃腸障害

NSAIDsは，胃・食道炎，粘膜潰瘍，出血，胃酸による潰瘍，消化管穿孔，閉塞といった幅広い範囲の胃腸障害を引き起こす[3]．NSAIDsの胃腸粘膜障害の発現機序は，①NSAIDsが直接胃粘膜バリアを破壊し，上皮細胞を傷害する局所作用，②胃腸粘膜保護作用を担うPG産生酵素COX-1阻害による粘膜防御機能の破綻，③NSAIDsによるフリーラジカル産生，などである．胃腸粘膜障害の自覚症状は，上腹部痛，心窩部痛が最も多く，次いで吐下血，嘔気・嘔吐，食欲不振，胃部不快感であるが，突然の吐下血や穿孔症状を呈するまで無症状のこともある．内視鏡所見では，病変は多発であることが多く，潰瘍，びらん，それらに出血を伴う．NSAIDsの静注や筋注においても，潰瘍が認められることから，NSAIDsの胃腸障害の主な発現機序は，全身投与により吸収された薬物が胃腸粘膜細胞のCOX-1を阻害し，PG産生を抑制することによると考えられている[4]．ほとんどのNSAIDsは，COX-1およびCOX-2ともに阻害し，胃腸粘膜のPG産生を抑制する．セレコキシブやエトドラクなどのCOX-2選択的阻害薬は，胃腸粘膜のPG産生抑制作用は確かに弱い．しかしながら，十分な鎮痛作用が認められるCOX-2選択的阻害薬の臨床用量では，COX-1も少なからず阻害する．American College of Gastroenterologyは，NSAIDsの胃腸障害発現の最も重要なリスクファクターとして，①60歳以上の高齢者，②潰瘍や出血といった胃腸障害の病歴を持つ患者，③通常よりも2倍以上の高用量の投与，④ステロイドとの併用，⑤抗凝固薬との併用の5つを挙げている[5]．高齢者や胃腸障害の病歴を持つ患者の場合は，吸収された後に肝臓で活性型に代謝されるため，胃腸障害が少ないプロドラッグやCOX-2選択性の高い薬物，副作用発現の比較的少ないプロピオン酸系のNSAIDsを選択する．また，PG製剤であるミソプロストール，十分量のH_2受容体拮抗薬，プロトンポンプ阻害薬の併用することにより，胃腸障害の発症率を軽減させることが必要である．

2）NSAIDsによる腎機能障害

NSAIDsは，血行動態を介した急性腎不全とネフローゼ症候群を伴った急性間質性腎不全を引き起こす[6]．腎臓のPGは，①腎臓の微小血管を拡張させ，腎血流量や腎糸球体濾過率（glomerular filtration rate：GFR）を上昇させる，②腎髄質の血流量を調節する，③遠位尿細管の緻密斑でレニン分泌を促進し，血管を収縮させ，血圧を上昇させる，④尿細管でNa^+と水の再吸収を抑制する，⑤抗利尿ホルモンであるバソプレシンの作用に拮抗し，水の再吸収を抑制するといった生理作用を有する．腎臓ではCOX-1は，輸入細動脈，輸出細動脈，髄質に流れる血管，集合管の血管内皮細胞に存在する．一方COX-2は，腎臓では血管平滑筋や緻密斑に常在し，レニン分泌の調節やNa再吸収，腎血流量やGFRを調節している．NSAIDsによる血行動態を介した急性腎不全は，腎血管拡張性のPG産生抑制による腎血流量の低下とGFRの急激な低下により引き起こされる．急性腎不全の主な症状は，浮腫，高血圧やアシドーシスである．一般に血中半減期の長い薬物にこの傾向が強いとされていることから，腎機能障害患者や高齢者，また心不全，肝硬変，脱水状態を有するハイリスク患者には，血中半減